Experimental and numerical investigation of the strain rate-dependent compression behaviour of a carbon-epoxy structure

Schmack, T.; Morgado Martins Filipe, T.M.; Deinzer, G.; Kassapoglou, C.; Walther, F.

DOI
10.1016/j.compstruct.2017.11.025

Publication date
2018

Document Version
Accepted author manuscript

Published in
Composite Structures

Journal Logo

Journal Name 00 (2018) 1–8

Experimental and numerical investigation of the strain rate-dependent compression behaviour of a carbon-epoxy structure

T. Schmack[a,c,*], T. Filipe[a,b], G. Deinzer[a], C. Kassapoglou[b], F. Walther[c]

[a] *Light Weight Center, Audi AG, NSU-Straße 1, 74148 Neckarsulm, Germany*
[b] *Department of Aerospace Structures & Materials, TU Delft, Kluyverweg 1, 2629 HS Delft, the Netherlands*
[c] *Department of Materials Test Engineering (WPT), TU Dortmund University, Baroper Str. 303, 44227 Dortmund, Germany*

Abstract

The usage of fibre-reinforced composites in automotive body structures is still a rarity. The main goal in body structure development is to design lightweight structures as cost-efficient as possible. This research contributes to the approach of maximal material usage by considering the strength increase of a carbon-epoxy laminate with increasing strain rate. The objective was to substantiate the well known material characteristic's strain rate dependency from a coupon level to realistic body structure component - experimentally and numerically. Hence, a special compression fixture was developed to obtain all necessary characteristic values of the investigated T700S DT120 prepreg system. The rectangular coupon specimens were loaded with quasi-static to intermediate strain rates (2×10^{-4} to 70 s^{-1}). A second compression fixture was developed to axially load omega cross-sectional specimens with strain rates ranging from 2×10^{-4} to 5 s^{-1}. The experimental tests showed a significant increase of +23% and +21% in compression strength for rectangular coupon specimens and omega cross-sectional components, respectively. Furthermore, the numerical simulation showed the same increase in strength of +21% for omega cross-sectional components. This work has proven the necessity of considering the strain rate dependency of a composite material to accurately predict the maximum load capacity of a structure during a dynamic load event like a crash.

Keywords: Carbon fibre, Epoxy, Prepreg, Strain rate, Compression strength, Finite Element Analysis

1. Introduction

With increasing usage of fibre-reinforced composites for structural components across the automotive and aerospace industry, it became crucial to understand how these materials behave when subjected to high loading rates, which are encountered in the case of crash events. In the past, structures were investigated based on their specific energy absorption (SEA) [1, 2, 3, 4]. Components within the car body responsible for structural integrity are not supposed to fail during a crash event. Hence, the maximal laminate strength and fracture strain is the design limiting parameter. Especially, the improved strength with increasing strain rate is a key factor to achieving maximal material usage. Consequently, for a proper numerical implementation and a good correlation between Finite Element Analysis (FEA) and experiments a holistic investigation of the characteristic of fibre-reinforced plastics (FRP) at different strain rates is mandatory.

The first results of dynamic tensile testing of unidirectional carbon-epoxy composites were published by Harding and Welsh [5], who used a tensile Split Hopkinson Pressure Bar (SHPB) and found no correlation between the tensile properties in fibre direction and the rate of loading. Similar results were found by Taniguchi et al. [6] for unidirectional T700S/2500 carbon-epoxy specimens at strain rates up to 100 s^{-1}. These results are in agreement with the tensile tests that Zhou et al. [7, 8] performed on carbon fibre bundles and found no change in the tensile properties of carbon fibres with varying strain rate.
Since the tensile properties of fibre-reinforced polymers loaded in fibre direction are fibre-dominated, it is comprehensible that the composite response at different strain rates is similar to the behaviour of carbon fibre bundles, i.e. not strain rate sensitive.

On the other hand, the mechanical response of a unidirectional composite when loaded in the direction transverse to the fibres is matrix-dominated. Gilat et al. [9] and Taniguchi et al. [6] performed dynamic tension tests on unidirectional carbon-epoxy laminates in transverse direction. Both studies found an increase in transverse tensile modulus and failure

*Corresponding author. *Tel.:* +49 152 32746082
Email address: tobias.schmack@audi.de (T. Schmack)

stress with increasing strain rate. The reported increase is in the order of 12.5% and 17.8% for the modulus and strength, respectively, between-quasi-static conditions and a strain rate of 100 s^{-1}.

If a longitudinal compression load is applied to a unidirectional carbon-epoxy laminate, the mechanical properties are dominated by the fibres. Therefore, one would expect these properties not to vary with increasing strain rate, since carbon fibres properties are not strain rate-dependent [7, 8].
However, the longitudinal compressive strength of fibre-reinforced polymers is intimately controlled by the matrix behaviour [10]. When loaded axially in compression, the fibres tend to micro-buckle and, consequently, create kink bands [11, 12, 13]. The matrix resin provides lateral support to the fibres, preventing them from buckling, up until the matrix reaches its yield point. If the resin material is strain rate-dependent and its yield point shifts with increasing strain rate, then it is expected that fibre microbuckling will occur at higher stress/strain levels when the material is loaded at higher rates.
An increase in failure strain and strength is described by several authors for unidirectional carbon-epoxy laminates under compression loading at high strain rates [14, 15, 16, 17, 18]. When testing at strain rates of approximately 100 s^{-1} the reported increase in most studies is in the order of 40% for both failure strain and strength, compared to the quasi-static value.

The compressive transverse properties of carbon-epoxy laminates are also matrix-dominated. Compression tests performed by Hsiao et al. [19] on [90°] specimens at strain rates of 1800 s^{-1} showed increases of 94% and 37% compared to the quasi-static values for the transverse compression strength and modulus, respectively. Similarly, Koerber et al. [20] report increases of 45% and 12% over the quasi-static values, when testing at strain rates of 270 s^{-1} for the transverse strength and modulus, respectively, which is in very good agreement with the previously presented results.

In accordance with tensile and compressive transverse properties, the shear properties are highly influenced by the matrix behaviour. Several authors have performed tension and compression dynamic tests on [+45°/ − 45°] carbon-epoxy specimens and found similar results: the shear modulus, strength and yield stress/strain increases significantly with increasing strain rate [6, 9, 21, 22, 23]. Other authors extrapolated the shear properties from off-axis testing of unidirectional laminates at varying strain rates [19, 20, 24] and found similar increases in shear modulus, strength and yielding properties for dynamic strain rates. The increase in laminate shear properties is consistent with the increase found in the shear properties of neat epoxy specimens tests at high strain rates [25, 26].

The objective of this work is to characterise the strain rate-dependent in plane compressive strength and stiffness of a carbon-epoxy laminate on coupon level. These experimentally obtained properties are then implemented in a commercially available finite-element package. In a first validation step the simulation laminate behaviour is compared with the experimental results. Furthermore, the analysis is then extended into a generic structural component, to examine if the strain rate dependency goes beyond a coupon level and into more complex structural components. For this purpose the numerical results are validated by experimental dynamic tests on omega profile cross-sectional components.

2. Materials and Specimen Preparation

2.1. Materials

The specimens manufactured consist of DT120 epoxy matrix by DeltaTech reinforced with high-strength standard-modulus T700S carbon fibres by Toray. The unidirectional prepreg tape is 0.15 *mm* thick and has a fibre areal weight of 150 g/m^2.

2.2. Rectangular cross-section specimens preparation

The plies were hand-laid as rectangular plates with dimensions of 500×600 mm^2 and cured in an autoclave for 1.5 hours at 120 °C. Nine Fibre Volume Content (FVC) measurements were performed for each plate, resulting in an average FVC of 53.5% ($\pm 0.3\%$). The cured plates were then equipped with 35 *mm* long loading tabs made of quasi-isotropic (QI) Glass Fibre Reinforced Plastic (GFRP) (2 *mm* thick) using DP490 Scotch-Weld epoxy adhesive by 3M. The individual specimens (Figure 1) were cut to the final dimensions of $12 \times 10 \times 2.4$ *mm* (width × gauge length × thickness) using a water-cooled rotating diamond saw. Specimens with three different layups were manufactured: $[0°]_{16}$, $[90°]_{16}$ and $[+45°/-45°]_{4s}$.

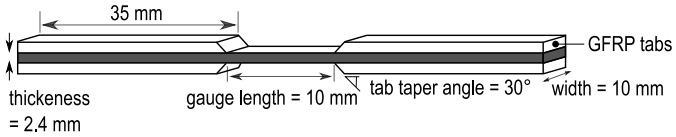

Figure 1: Rectangular specimens geometry and dimensions.

2.3. Omega-profile cross-section specimens preparation

The second type of samples manufactured consists of 100 *mm* long omega-profile cross-section specimens. The prepreg system used is identical to the previously mentioned one. The individual unidirectional layers were hand-laid with a $[45°/-45°/45°/-45°/0°/90°]_s$ layup on a concave omega-shape mould and cured also at 120 °C for 1.5 hours, resulting in the specimen dimensions shown in Figure 2 (after trimming).

3. Experimental Setup

For this work, the purpose was to study the compressive behaviour of carbon-epoxy laminates subjected to strain rates varying from the typical quasi-static values (order of magnitude 10^{-5} s^{-1}) to moderate (up to 100 s^{-1}). Therefore, the static and dynamic tests were performed on a Very High Speed (VHS) Instron servo-hydraulic testing machine, using a displacement

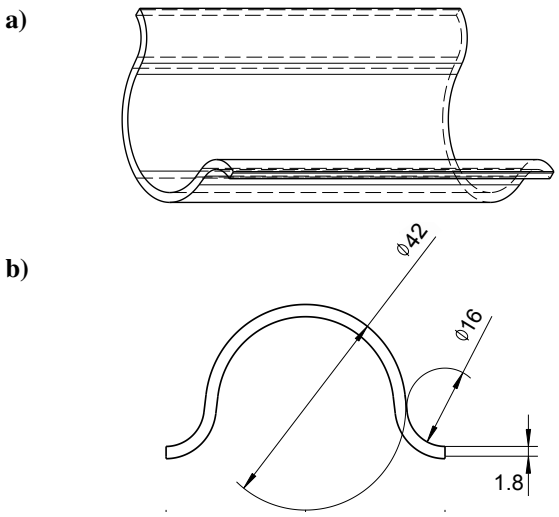

Figure 2: Omega cross-sectional component. **a)** Isometric view, **b)** Cross-section view.

controlled vertical shaft. Using the same testing machine across the entire considered range of strain rates ensures that the effect of the fixture/machine on the measured results are constant.

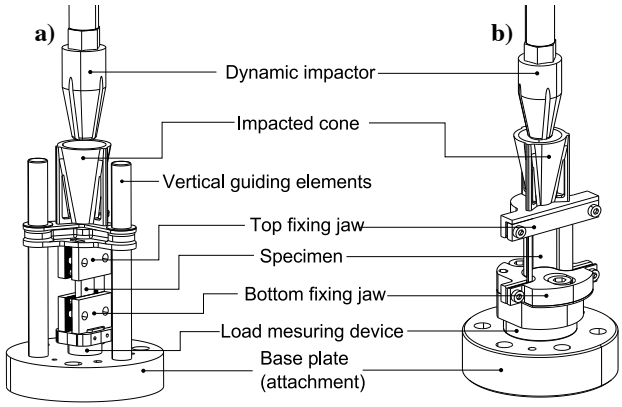

Figure 3: Self developed compression fixtures for a) rectangular and b) omega profile specimens

Two fixtures were developed to clamp the two different specimen shapes. However, a special attention was placed when designing the two fixtures to ensure that their effect on the specimens is as similar as possible. Figure 3 shows the two fixture configurations: rectangular cross-section specimens (a) and omega-profile cross-section specimens (b). Both fixtures introduce the load via end loading and via shear through the fixing jaws, reducing the stress concentration factor at the clamps and preventing specimen crush. The load applied on the specimen is measured using a piezoelectric load cell (Kistler 9051A for the rectangular cross-secion specimen and Kistler 9071A for the omega-profile cross-section specimens) mounted on the fixture base.

The specimen strain is measured using the Digital Image Correlation (DIC) software ARAMIS® supplied by Gesellschaft für optische Messtechnik (GOM), together with two Photron FASTCAM SA-X high-speed cameras.

4. Experimental Results

4.1. Rectangular cross-section specimens

Specimens with $[0°]_{16}$, $[90°]_{16}$ and $[+45°/-45°]_{4s}$ layup were experimentally tested at six different impactor velocities (which develops into specimen deformation speed), ranging from 2 mm/min to 1 m/s. For each combination of specimen layup and impactor speed, ten replicated experiments were performed to ensure an appropriate average accuracy.
For the tests performed in fibre direction ($[0°]_{16}$ layup), the strain rates achieved ranged between 2.3×10^{-4} and 4 s^{-1}. Throughout this range, the longitudinal modulus does not show significant changes. On the other hand, the compression strength and fracture strain increase by 22% and 26%, respectively. Figure 4 **(a)** depicts the average longitudinal stress-strain curves obtained at each of the six loading rates tested, with the in-fibre direction compression properties being summarized in Table 1.

Table 1: Averaged longitudinal compression properties ($[0°]_{16}$ layup specimens).

Strain Rate $\dot{\varepsilon}$ [s^{-1}]	Strength [MPa]	Fracture Strain [%]	Longitudinal Modulus [GPa]
$2.3 \pm 0.1 \times 10^{-4}$	1165 ± 10	1.15 ± 0.03	104.9 ± 2.2
$7.2 \pm 0.5 \times 10^{-4}$	1215 ± 45	1.18 ± 0.06	112.8 ± 2.1
$7.6 \pm 0.4 \times 10^{-3}$	1288 ± 10	1.29 ± 0.04	106.9 ± 3.0
$7.4 \pm 0.5 \times 10^{-2}$	1352 ± 25	1.33 ± 0.05	110.1 ± 3.5
$6.6 \pm 0.4 \times 10^{-1}$	1380 ± 13	1.36 ± 0.05	111.8 ± 2.9
4.1 ± 0.5	1422 ± 33	1.45 ± 0.06	111.2 ± 2.7

In transverse direction ($[90°]_{16}$ layup), higher strain rates were achieved, resulting in a range between 2.9×10^{-3} and 70 s^{-1}. Both the transverse fracture strain and modulus are unaffected by the deformation rate, as they are kept more or less constant at 5.2% ±0.18 % and 8.4 GPa ±0.07 GPa, respectively. Nonetheless, there is a significant increase in yield and fracture stress, as high as 56% for both these properties. With increasing strain rate, the transverse response of the carbon-epoxy laminate becomes more brittle, with yielding and failure occurring at higher stress levels, as shown by the transverse stress-strain curves of Figure 4 **(b)**. Detailed results are given in Table 2.

The shear properties are also affected by the deformation rate, as verified when testing $[+45°/-45°]_{4s}$ layup specimens in strain rates ranging from 6.2×10^{-3} to 70 s^{-1}. Similarly to the longitudinal and transverse moduli, the shear modulus does not seem to change with increasing rates. Nonetheless, the shear yield stress and strength (defined as the shear stress when the shear strain reaches 5%) increase by 37% and 27%, respectively. Figure 4 **(c)** shows the shear stress-strain curves

obtained at the different strain rates tested, with the main shear properties being summarized in Table 3.

4.2. *Omega-profile cross-section specimens*

Impact test with impactor velocities of 3.3×10^{-5} m/s, 0.01 m/s and 1 m/s were performed with omega-profile cross-sectional specimens. For each speed, three replicated experiments were carried out.

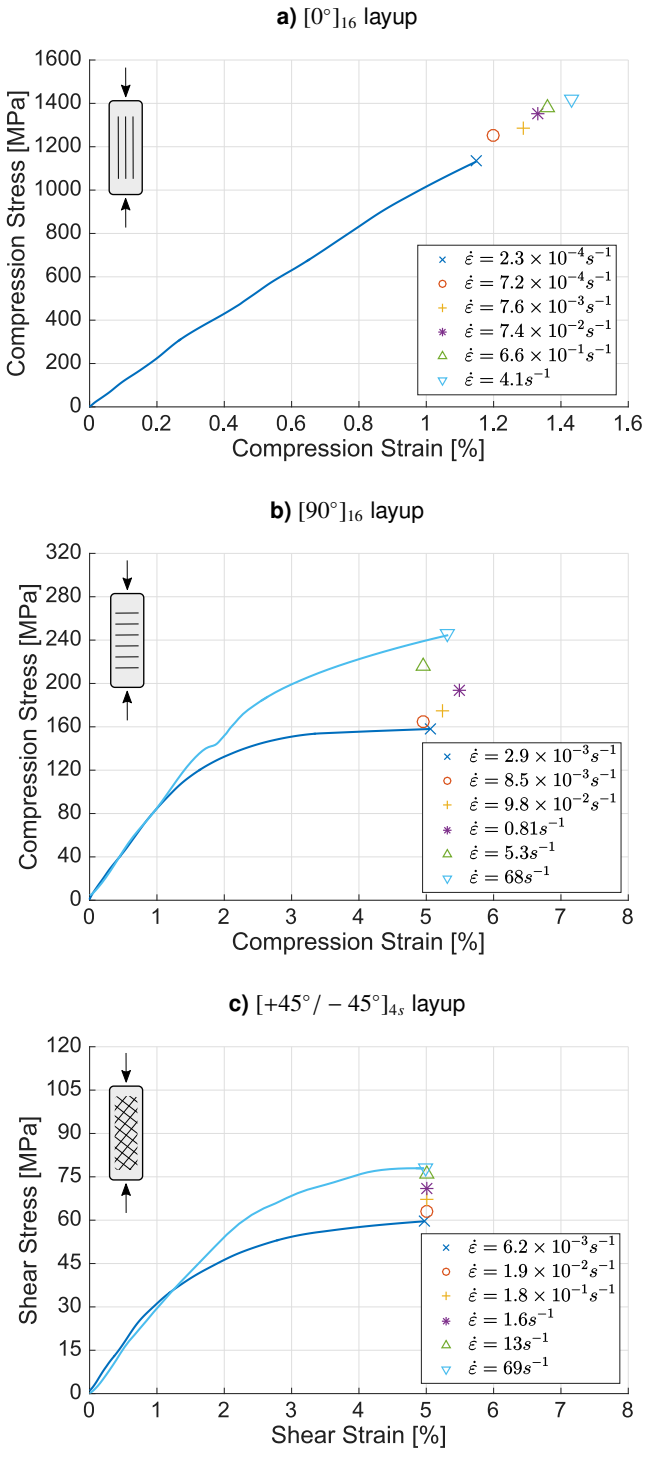

Figure 4: Stress-strain curves of rectangular specimens.

Table 2: Averaged transversal compression properties ($[90°]_{16}$ layup specimens).

Strain Rate $\dot{\varepsilon}$ $[s^{-1}]$	Strength [MPa]	Fracture Strain [%]	Yield Stress [MPa]	Transverse Modulus [GPa]
$2.9 \pm 0.5 \times 10^{-3}$	158 ± 5	5.05 ± 0.52	113 ± 2	8.53 ± 0.22
$8.5 \pm 0.8 \times 10^{-3}$	165 ± 4	4.96 ± 0.44	117 ± 1	8.59 ± 0.16
$9.8 \pm 1.1 \times 10^{-2}$	175 ± 4	5.24 ± 0.43	114 ± 3	8.70 ± 0.20
$8.1 \pm 1.0 \times 10^{-1}$	194 ± 4	6.11 ± 0.47	136 ± 2	8.22 ± 0.14
5.3 ± 0.6	216 ± 3	4.60 ± 0.26	159 ± 8	8.32 ± 0.25
68 ± 10	247 ± 2	5.31 ± 0.45	177 ± 8	8.29 ± 0.27

Table 3: Averaged shear layup properties ($[+45°/-45°]_{4s}$).

Strain Rate $\dot{\varepsilon}$ $[s^{-1}]$	Stress at 5% Strain [MPa]	Yield Shear Stress [MPa]	Shear Modulus [GPa]
$6.2 \pm 0.1 \times 10^{-3}$	60.0 ± 0.2	35.4 ± 0.4	3.49 ± 0.05
$1.9 \pm 0.1 \times 10^{-2}$	63.1 ± 0.3	37.1 ± 0.4	3.78 ± 0.06
$1.8 \pm 0.1 \times 10^{-1}$	67.2 ± 0.4	38.5 ± 0.5	3.70 ± 0.06
1.6 ± 0.1	70.9 ± 0.4	40.3 ± 0.5	3.73 ± 0.06
13 ± 1	76.8 ± 0.2	41.0 ± 1.2	3.75 ± 0.12
69 ± 4	76.3 ± 0.8	48.5 ± 2.0	3.51 ± 0.07

With increasing deformation rate, the maximum cross-section load sustained by the specimens increased from 55.6 kN to 67.3 kN, which represents an increase of 21%. This growth in strength is in line with the increase previously presented for rectangular specimens with a $[0°]_{16}$ layup, as the 0° plies are the main load-carrying plies of the omega-profile cross-section specimens. Figure 5 shows the piston displacement vs. compression force for the nine specimens tested. It is relevant to note the inconsistency in impactor displacement at failure between the three testing velocities, which is related with fixture and testing machine limitations, allowing the specimens to slightly move inside the fixing jaws. For this reason, the impactor displacement after impact does not translate directly into specimen strain. Table 4 summarizes the failure strain and maximum load for the three different testing velocities considered.

Table 4: Averaged strain rate, maximum load and failure strain for the axially loaded omega profiles

Impactor Velocity $[m/s]$	Strain Rate $(\dot{\varepsilon})$ $[s^{-1}]$	Maximum Load $[kN]$	Strain at Failure [%]
3.3×10^{-5}	$1.9 \pm 0.2 \times 10^{-4}$	55.6 ± 1.6	1.21 ± 0.06
1×10^{-2}	$5.3 \pm 0.4 \times 10^{-2}$	60.3 ± 2.0	1.34 ± 0.07
1	4.7 ± 0.2	67.3 ± 1.0	1.42 ± 0.03

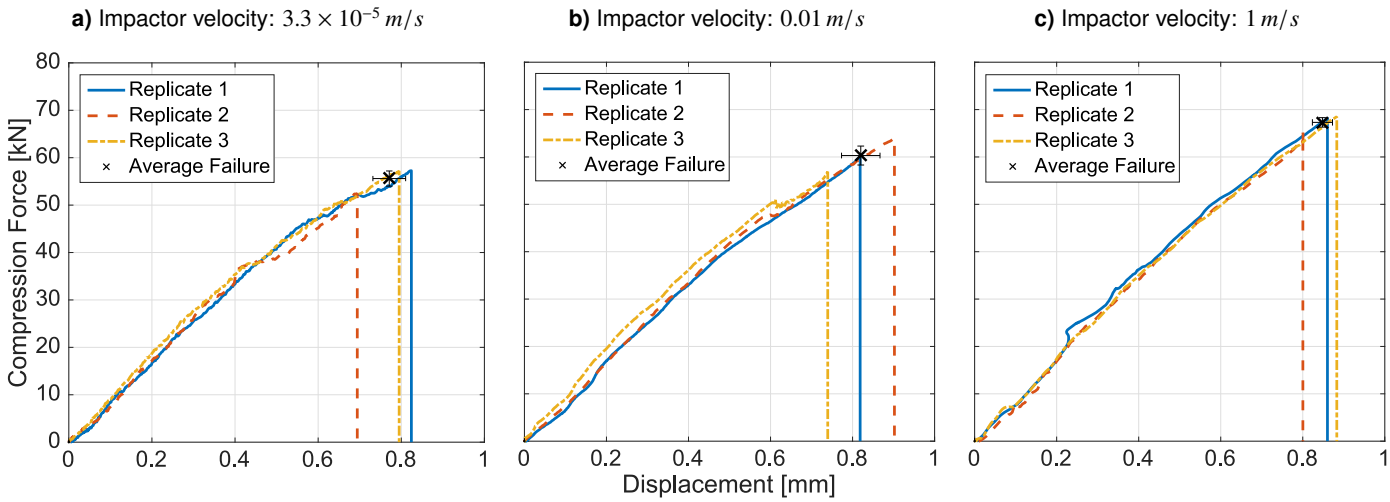

Figure 5: Omega-shape experimental tests: piston displacement vs. compression force.

5. Numerical Model Implementation

The simulations were carried out using the commercially available explicit Finite Element software Pam-Crash from ESI. The laminate was modelled using Mindlin plate theory shell elements and the ply mechanics are based on a continuum damage approach proposed by Ladeveze and Le Dantec [27]. The strain rate dependency is based on the work of Rozycki [28] and it consists of using viscosity functions to describe the variation of the ply properties with the strain rate. As was experimentally verified, neither the longitudinal, transverse or shear moduli are affected by the deformation rate. Therefore, the ply behaviour can be modelled by using only two viscosity functions - also denoted functions of evolution.

5.1. Strain rate dependency of longitudinal fracture strain

The compressive fracture strain in fibre direction $\varepsilon^c_{1,fail}$ increases linearly with the logarithm of the strain rate, as Figure 6 **(a)** shows. Therefore, a logarithmic function describes accurately the increase in longitudinal fracture strain with increasing strain rate:

$$\varepsilon^c_{1,fail} = \begin{cases} 1.15\ [\%] & \text{if} \quad \dot{\varepsilon} < 2.3 \times 10^{-4}\ s^{-1} \\ 1.15 \times \left[1 + 0.0262 \ln\left(\dfrac{\dot{\varepsilon}}{2.3 \times 10^{-4}}\right)\right][\%] & \text{if} \quad 2.3 \times 10^{-4} \leqslant \dot{\varepsilon} \leqslant 4.1\ s^{-1} \\ 1.45\ [\%] & \text{if} \quad \dot{\varepsilon} > 4.1\ s^{-1} \end{cases}$$

Below the lowest strain rate tested, it is assumed that the failure strain is constant and equals the value obtained at the slowest performed test. In the range of deformation rates tested, the longitudinal fracture strain increases logarithmically between 1.15% and 1.45%. For strain rates higher than 4 s^{-1}, it is assumed that the failure strain does not increase any further, to prevent over estimations.

The implemented increase in fracture strain is accompanied by a similar increase in longitudinal ply compression strength, as the modulus is kept constant throughout the range of rates tested.

a) Evolution of longitudinal compression fracture strain with increasing strain rate derived from a $[0°]_{16}$ laminate.

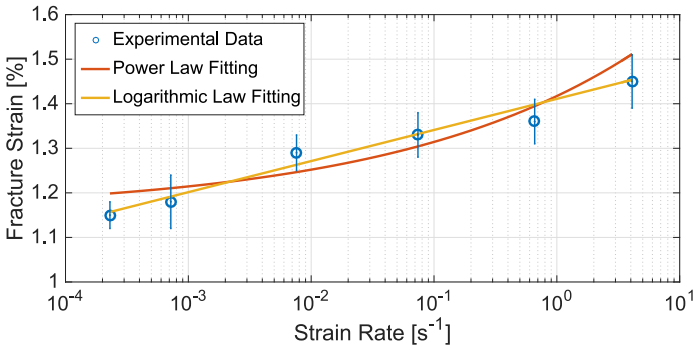

b) Evolution of yield stress with increasing strain rate derived from a $[90°]_{16}$ laminate.

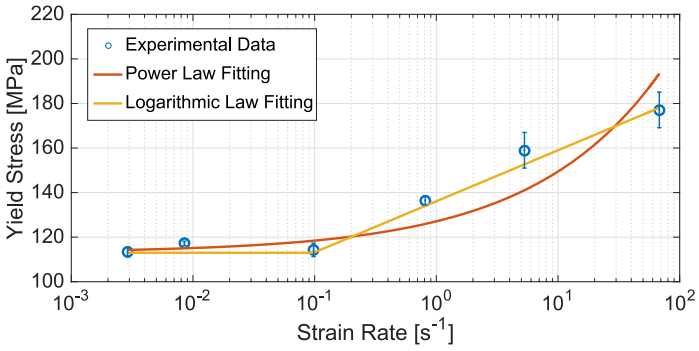

Figure 6: Experimental data described by a logarithmic and power law fit

5.2. Strain rate dependency of transverse yield stress

Similarly, the transverse yield stress R_0 obtained from tests in transverse direction ($[90°]_{16}$ layup) also increases linearly with the logarithm of the strain rate, above a certain threshold, as shown in Figure 6 **(b)**. Therefore, the growth in yield stress as function of the strain rate can be expressed and implemented in the numerical model as:

$$R_0 = \begin{cases} 113 \text{ [MPa]} & \text{if} \quad \dot{\varepsilon} < 10^{-1}\ s^{-1} \\ 113 \times \left[1 + 0.088 \ln\left(\dfrac{\dot{\varepsilon}}{10^{-1}}\right)\right] \text{[MPa]} & \text{if} \quad 10^{-1} \leqslant \dot{\varepsilon} \leqslant 68\ s^{-1} \\ 180 \text{ [MPa]} & \text{if} \quad \dot{\varepsilon} > 68\ s^{-1} \end{cases}$$

6. Numerical Simulation Results and Comparison

6.1. Numerical model validation

Calibration and validation of the implemented numerical model was carried out by comparing the experimental tests using rectangular specimens with the simulation response of a single shell element model.

In fibre direction, the simulation stress-strain curves match quite accurately the experimental data obtained, as shown in Figure 7 **(a)**, since both the failure strain and compression strength increase equally with increasing strain rate.

In the ply transverse direction, the varying yield stress with changing strain rate is implemented quite accurately, but the simulation stress-strain curves after yielding do not follow the exact same development as the experimental ones. This discrepancy is related with the alteration of the hardening law with varying strain rates observed experimentally, which was not implemented in the numerical model. This divergence results in the simulations overpredicting the strength at low strain rates and underpredicting at higher deformation rates, as depicted in Figure 7 **(b)**.

The simulation shear response is satisfactory, as it correlates quite well with the experimentally obtained stress-strain curves (Figure 7 **(c)**). The simulation shear stress levels at 2.5% and at 5% shear strain matches the experimental data with an error below 5%, which indicates a quite good correlation between experiments and simulations.

6.2. Omega-profile cross-section specimen simulations

A simulation model that depicts the experimental crash tests performed with an omega-profile cross-section structural component was developed using the previously implemented and verified numerical model. The simulation impact velocity was chosen such that the strain rate achieved is analogous to the experimentally obtained one. Figure 8 shows the displacement vs. compression force resulting from running the simulation model at the three indicated strain rates.

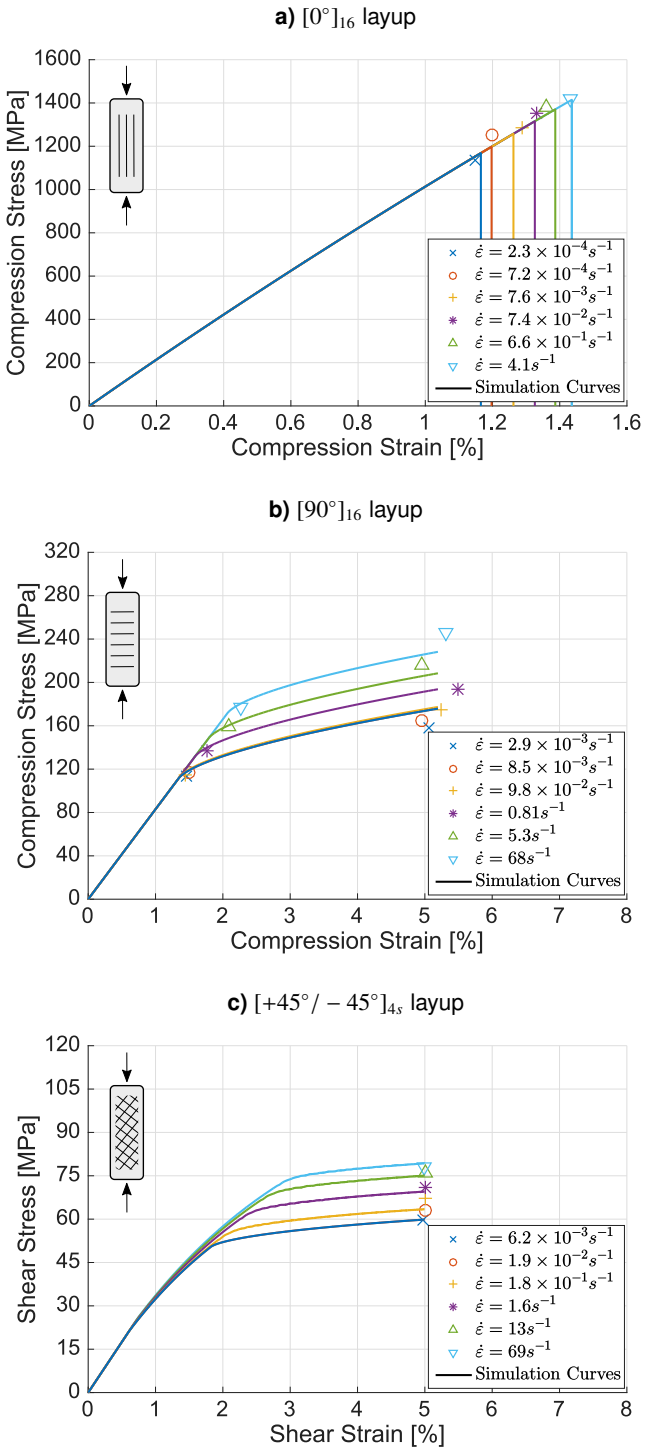

Figure 7: Experimental and simulation stress-strain curves (rectangular specimens).

Similarly to the analogous experimental curves shown in Figure 5, the force-displacement graphs are linear until failure, where the cross-section force immediately drops to zero. The fact that there is no drop in the component stiffness signifies that there is no manifestation of buckling, crippling or any other failure phenomenon related with the specimen geometry. The sudden drop in cross-sectional force indicates that failure oc-

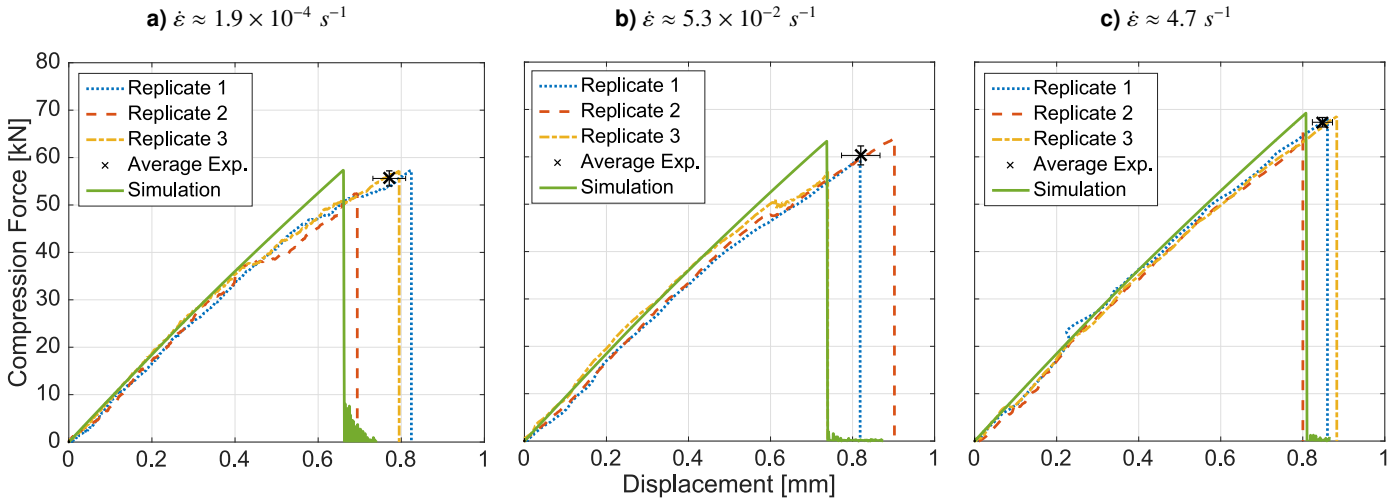

Figure 8: Experimental and simulation displacement vs. force curves (omega-profile specimens).

Table 5: Experimental and simulation comparison of maximum load and failure strain of the omega-profile

Strain Rate	Maximum Load			Strain at Failure		
	Exp.	Sim.	Error	Exp.	Sim.	Error
$\dot{\varepsilon}$ [s^{-1}]	[kN]	[kN]	[%]	[%]	[%]	[%]
1.9×10^{-4}	55.6	57.3	+2.9	1.21	1.10	-10
5.3×10^{-2}	60.3	63.3	+4.7	1.34	1.23	-8.9
4.7	67.3	69.2	+2.7	1.42	1.35	-5.2

curs due to material failure, which in the simulation is seen as elements being eliminated due to their longitudinal maximum allowed strain being reached. Table 5 contains a comparison between the experimentally and numerically obtained maximum load and failure strain, at the three different strain rate levels tested.

The numerical model is able to predict the maximum load quite accurately, since the relative error is kept below 5% for the three testing velocities considered. Furthermore, the increase in maximum load with increasing deformation rates is implemented in a quite satisfactory way.

7. Conclusions

The first conclusions that can be drawn are related to the results of the experimental tests performed and the strain rate-dependent compression properties of the considered T700-DT120 carbon-epoxy system. With increasing strain rates, the longitudinal strength and failure strain increase logarithmically with the strain rate, reaching growths up to approximately 25% for the range of deformation rate considered. The matrix-dominated properties of the laminate increase further, with the transverse yield and ultimate stress growing by 56% over the respective quasi-static values, when tested at a strain rate of 70 s^{-1}.

This dependency of the material response on the deformation rate was also observed for specimens with an omega cross-section geometry. The experimental impact tests on specimens with an omega-profile cross-section show an increase in maximum compression force analogous to the previously registered for unidirectional rectangular specimens tested longitudinally. The maximum cross-sectional force supported by this component increased by 21% from quasi-static tests at a strain rate of $2 \times 10^{-4}\ s^{-1}$ to dynamic tests at a strain rate 5 s^{-1}.

Multidirectional laminates can be seen as structures, whose response highly depends not only on the behaviour of the individual ply, but also on the stacking order. Since the strength increase observed in unidirectional rectangular specimens (+25%) tested longitudinally is in line with the increase in maximum force registered for the omega-profile cross-section specimen with a multidirectional layup (+21%), it can be concluded that the material and structural response are quite similar. Therefore, simple rectangular specimens can be used to characterise the material behaviour, and these properties can be extended and used to predict the response of scaled-up structural components.

Finally, the strain rate-dependent compression properties were implemented on a numerical model, resulting in satisfactory predictions of the experimental impact tests across the entire range of deformation rate considered, for both rectangular and omega-profile cross-section specimen types.

Acknowledgements

The authors gratefully acknowledge the support of Audi AG lightweight design team, in particular, M.H. Kothmann, J. Rausch and D. Roquette for proofreading and supporting the research activities. Furthermore we thank D. Huelsbusch for his support.

References

[1] J. Meredith, E. Bilson, R. Powe, E. Collings, K. Kirwan, A performance versus cost analysis of prepreg carbon fibre epoxy energy absorption structures, Composite Structures 124 (2015) 206–213. doi:10.1016/j.compstruct.2015.01.022.
URL 10.1016/j.compstruct.2015.01.022

[2] G. Belingardi, H. Mehdipour, E. Mangino, B. Martorana, Progressive damage analysis of a rate-dependent hybrid composite beam, Composite Structures 154 (2016) 433–442. doi:10.1016/j.compstruct.2016.07.055.
URL 10.1016/j.compstruct.2016.07.055

[3] S. Fischer, A material model for fe-simulation of ud composites, Applied Composite Materials 23 (2) (2016) 197–217. doi:10.1007/s10443-015-9456-1.
URL 10.1007/s10443-015-9456-1

[4] Q. Liu, H. L. Xing, Y. Ju, Z. Y. Ou, Q. Li, Quasi-static axial crushing and transverse bending of double hat shaped cfrp tubes, Composite Structures 117 (2014) 1–11. doi:10.1016/j.compstruct.2014.06.024.
URL 10.1016/j.compstruct.2014.06.024

[5] J. Harding, L. M. Welsh, A tensile testing technique for fiber-reinforced composites at impact rates of strain, Journal of Materials Science 18 (6) (1983) 1810–1826. doi:10.1007/Bf00542078.
URL 10.1007/Bf00542078

[6] N. Taniguchi, T. Nishiwaki, H. Kawada, Tensile strength of unidirectional cfrp laminate under high strain rate, Advanced Composite Materials 16 (2) (2007) 167–180. doi:10.1163/156855107780918937.
URL 10.1163/156855107780918937

[7] Y. X. Zhou, D. Z. Jiang, Y. M. Xia, Tensile mechanical behavior of t300 and m40j fiber bundles at different strain rate, Journal of Materials Science 36 (4) (2001) 919–922. doi:10.1023/A:1004803202658.
URL 10.1023/A:1004803202658

[8] Y. X. Zhou, Y. Wang, Y. M. Xia, S. Jeelani, Tensile behavior of carbon fiber bundles at different strain rates, Materials Letters 64 (3) (2010) 246–248. doi:10.1016/j.matlet.2009.10.045.
URL 10.1016/j.matlet.2009.10.045

[9] A. Gilat, R. K. Goldberg, G. D. Roberts, Experimental study of strain-rate-dependent behavior of carbon/epoxy composite, Composites Science and Technology 62 (10-11) (2002) 1469–1476. doi:10.1016/S0266-3538(02)00100-8.
URL 10.1016/S0266-3538(02)00100-8

[10] I. M. Daniel, H. M. Hsiao, S. C. Wooh, Failure mechanisms in thick composites under compressive loading, Composites Part B-Engineering 27 (6) (1996) 543–552. doi:10.1016/1359-8368(95)00010-0.
URL 10.1016/1359-8368(95)00010-0

[11] J. Lee, C. Soutis, A study on the compressive strength of thick carbon fibre-epoxy laminates, Composites Science and Technology 67 (10) (2007) 2015–2026. doi:10.1016/j.compscitech.2006.12.001.
URL 10.1016/j.compscitech.2006.12.001

[12] A. Jumahat, C. Soutis, F. R. Jones, A. Hodzic, Fracture mechanisms and failure analysis of carbon fibre/toughened epoxy composites subjected to compressive loading, Composite Structures 92 (2) (2010) 295–305. doi:10.1016/j.compstruct.2009.08.010.
URL 10.1016/j.compstruct.2009.08.010

[13] Q. Bing, C. T. Sun, Specimen size effect in off-axis compression tests of fiber composites, Composites Part B-Engineering 39 (1) (2008) 20–26. doi:10.1016/j.compositesb.2007.02.010.
URL 10.1016/j.compositesb.2007.02.010

[14] H. M. Hsiao, I. M. Daniel, Strain rate behavior of composite materials, Composites Part B-Engineering 29 (5) (1998) 521–533. doi:10.1016/S1359-8368(98)00008-0.
URL 10.1016/S1359-8368(98)00008-0

[15] H. Koerber, P. P. Camanho, High strain rate characterisation of unidirectional carbon-epoxy im7-8552 in longitudinal compression, Composites Part A: Applied Science and Manufacturing 42 (5) (2011) 462–470. doi:10.1016/j.compositesa.2011.01.002.
URL 10.1016/j.compositesa.2011.01.002

[16] M. V. Hosur, J. Alexander, U. K. Vaidya, S. Jeelani, High strain rate compression response of carbon/epoxy laminate composites, Composite Structures 52 (3-4) (2001) 405–417. doi:10.1016/s0263-8223(01)00031-9.
URL 10.1016/s0263-8223(01)00031-9

[17] Q. D. Bing, C. T. Sun, Modeling and testing strain rate-dependent compressive strength of carbon/epoxy composites, Composites Science and Technology 65 (15-16) (2005) 2481–2491. doi:10.1016/j.compscitech.2005.06.012.
URL 10.1016/j.compscitech.2005.06.012

[18] T. Schmack, D. Huelsbusch, R. Righi, J. Rausch, D. Roquette, G. Deinzer, F. Walther, Influence of load application and fixture on characteristic values at short-time dynamic compression testing of carbon fibre-epoxy composites, Paper Presented at the 17th European Conference on Composite Materials.

[19] H. M. Hsiao, I. M. Daniel, R. D. Cordes, Strain rate effects on the transverse compressive and shear behavior of unidirectional composites, Journal of Composite Materials 33 (17) (1999) 1620–1642.

[20] H. Koerber, J. Xavier, P. P. Camanho, High strain rate characterisation of unidirectional carbon-epoxy im7-8552 in transverse compression and in-plane shear using digital image correlation, Mechanics of Materials 42 (11) (2010) 1004–1019. doi:10.1016/j.mechmat.2010.09.003.
URL 10.1016/j.mechmat.2010.09.003

[21] G. H. Staab, A. Gilat, High-strain rate response of angle-ply glass epoxy laminates, Journal of Composite Materials 29 (10) (1995) 1308–1320.

[22] M. M. Shokrieh, M. J. Omidi, Compressive response of glass-fiber reinforced polymeric composites to increasing compressive strain rates, Composite Structures 89 (4) (2009) 517–523. doi:10.1016/j.compstruct.2008.11.006.
URL 10.1016/j.compstruct.2008.11.006

[23] H. Cui, D. Thomson, A. Pellegrino, J. Wiegand, N. Petrinic, Effect of strain rate and fibre rotation on the in-plane shear response of ±45° laminates in tension and compression tests, Composites Science and Technology 135 (2016) 106–115. doi:10.1016/j.compscitech.2016.09.016.
URL 10.1016/j.compscitech.2016.09.016

[24] J. L. Tsai, C. T. Sun, Strain rate effect on in-plane shear strength of unidirectional polymeric composites, Composites Science and Technology 65 (13) (2005) 1941–1947. doi:10.1016/j.compscitech.2005.01.013.
URL 10.1016/j.compscitech.2005.01.013

[25] A. Gilat, R. K. Goldberg, G. D. Roberts, Strain rate sensitivity of epoxy resin in tensile and shear loading, Journal of Aerospace Engineering 20 (2) (2007) 75–89. doi:10.1061/(Asce)0893-1321(2007)20:2(75).
URL 10.1061/(Asce)0893-1321(2007)20:2(75)

[26] J. D. Littell, C. R. Ruggeri, R. K. Goldberg, G. D. Roberts, W. A. Arnold, W. K. Binienda, Measurement of epoxy resin tension, compression, and shear stress-strain curves over a wide range of strain rates using small test specimens, Journal of Aerospace Engineering 21 (3) (2008) 162–173. doi:10.1061/(Asce)0893-1321(2008)21:3(162).
URL 10.1061/(Asce)0893-1321(2008)21:3(162)

[27] P. Ladeveze, E. Ledantec, Damage modeling of the elementary ply for laminated composites, Composites Science and Technology 43 (3) (1992) 257–267. doi:10.1016/0266-3538(92)90097-M.
URL 10.1016/0266-3538(92)90097-M

[28] M. P. Rozycki, Contribution au developpement de lois de comportement pour materiaux composites soumis a l'impact, Phd thesis (2000).